A Particle-Augmented Mixed Lubrication Modeling Approach to Predicting Chemical Mechanical Polishing

Elon J. Terrell[1] and C. Fred Higgs III[2]
Carnegie Mellon University
Mechanical Engineering Department
Pittsburgh, PA. 15217

Abstract

Chemical mechanical polishing (CMP) is a manufacturing process that is commonly used to planarize integrated circuits and other small-scale devices during fabrication. Although a number of models have been formulated which focus on specific aspects of the chemical mechanical polishing (CMP) process, these models typically do not integrate all of the predominant mechanical aspects of CMP into a single framework. Additionally, the use of empirical fitting parameters decreases the generality of existing predictive CMP models. Therefore, the focus of this study is to develop an integrated computational modeling approach that incorporates the key physics behind CMP without using empirical fitting parameters. CMP consists of the interplay of four key tribological phenomena — the fluid mechanics, particle dynamics, contact mechanics, and resulting wear. When these physical phenomena are all actively engaged in a sliding contact, the authors call this particle augmented mixed lubrication (PAML). By considering all of the PAML phenomena in modeling particle-induced wear (or material removal), this model was able to predict wear *in silico* from a measured surface topography during CMP. The predicted material removal rate (MRR) was compared to experimental measurements of copper CMP. Parametric studies varying slurry properties, such as the solid fraction and abrasive particle size were also conducted. The results from the model are promising and suggest that a tribological framework is in place for developing a generalized first-principle PAML modeling approach for predicting CMP.

Accepted for Publication in the *ASME Journal of Tribology*, 2008

---

[1] Currently at Columbia University.

[2] Corresponding author: higgs@andrew.cmu.edu

Keywords: Mixed lubrication, chemical mechanical polishing, contact mechanics, particle dynamics, computational fluid dynamics, abrasive wear.

1. Introduction

In mixed lubrication, the load is supported by both the surface asperities and the interfacial fluid by way of its hydrodynamic pressure. When particles are introduced into a mixed-lubricated sliding contact, as shown in Fig. 1, the tribological regime can be called "particle- augmented mixed lubrication" (PAML). PAML can exist in numerous applications where there is partial contact of sliding surfaces and particulate-fluids, namely chemical mechanical polishing (CMP).

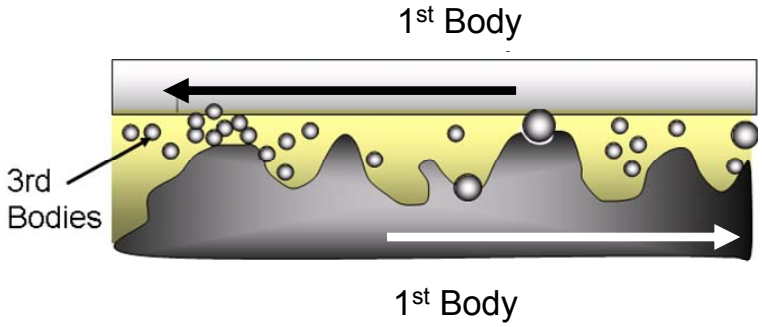

Figure 1: Diagram of particle-augmented mixed lubrication (PAML)

CMP has evolved into a critical fabrication step for planarizing semiconductor and other small scale devices due to the increasing demand for complex, multilevel devices. The CMP process involves the wafer sample being mounted onto a rotating carrier and pressed against a rotating polyurethane pad that is flooded with slurry. The slurry itself is a chemically reactive fluid containing suspended abrasive particles that serve as polishing agents.

Although the CMP process is widely used in industry, it can oftentimes produce unexpected results, which gives rise to the need for predictive CMP models. From a review of literature, it can be found that a number of CMP models have been developed for predicting various aspects of CMP. Nanz and Camilletti [1] have conducted an

extensive review of CMP wear models up until 1995, and more recently, Zantye et al. [2] performed a review of CMP models in the context of microelectronics fabrication. A number of CMP models were developed from a contact mechanics perspective, with the most general of the contact models analyzing surface wear on the wafer-scale using various semblances of Preston's equation [3, 4]. Some of the contact-based CMP models have also used statistical methods to account for the abrasive effect of the slurry particles [5-9]. However, the wafer-scale CMP models lack the ability to predict the occurrences of discrete wear events in CMP, such as dishing, erosion, and microscratching. Thus, other contact-based CMP models have been formulated to predict wear on the die-scale [10] and feature-scale [11]. Even at smaller scales, most of these models rely upon empirical formulations, such as Preston's equation applied on the asperity scale, for their predictions. Many CMP models have focused on analyzing the slurry fluid flow in the wafer-pad gap by modeling the hydrodynamic pressure distribution and flowfield [12]. Studies by Runnels [13] and Yao et al. [14] have even related the slurry shear rate to wafer surface wear. Higgs et al. [15] took a mixed lubrication approach to modeling CMP, in which both the contact mechanics and slurry fluid mechanics were integrated into the model. Also, a few studies exist that analyze the motion of the particles in the slurry both in CMP [16] and in other tribological geometries such as hard disk drives [17-19].

Although many models have been developed for predicting CMP, it has been found that each of them focused on one or two aspects of the CMP process, rather than integrating all of the key phenomena together into a single modeling framework. In addition, many of the models use empirical equations, such as the Preston equation applied on the wafer-scale or feature-scale, to predict wear. This approach may overlook much of the important physical phenomena within CMP, such as the slurry fluid flow and particle-induced wear, primarily through the use of an all-encompassing wear coefficient. The empirical wear formulation both limits the robustness of the model and also increases the uncertainty of the predictions. Therefore, the focus of this study involves the development of a multi-physics modeling tool that incorporates all of the important mechanical interactions in CMP—namely fluid mechanics, contact mechanics, and

particle dynamics—into a single computational framework. The resulting model makes predictions *in silico* by time-marching the physics in approximately the same way as the physical process [20]. This PAML-based wear approach to modeling CMP was used to predict the surface wear of an actual sample topography that was measured and input into the model. The predicted MRR from the PAML simulations was compared to the MRR from CMP experiments.

2. A Deterministic Approach to Representing Real Surfaces

Because of the complexity of developing a multi-physics PAML model, this study was framed to take advantage of the laboratory environment to reduce uncertainty in model variables. For example, the wafer surfaces being worn in the CMP tests were represented deterministically using their exact surface topography, as opposed to statistical representations (e.g., average roughness, rms roughness, skew, etc.). While this may not be practical in manufacturing where millions of wafers are processed, the aim of this work is to analyze the effectiveness of the PAML problem by making the input variables as close to the actual CMP test conditions as possible and consequently reducing parameter uncertainty.

Thus, two key inputs of the PAML model are the actual topographies of the two contacting surfaces, which are the wafer and the pad in the case of CMP. In order to facilitate the contact mechanics and wear modeling, the PAML model represents the wafer topography data as volume pixels, or voxels, where the asperities of surfaces are approximated as square-faced cuboids. Figure 2a shows the surface topography that was used in this study, which was measured using contact profilometry with a nanoindenter. Figure 2b shows the same surface represented as a series of voxels after being integrated into the PAML code. The frontal contact area of each voxel is given by

$$A_{voxel} = \left(\frac{L}{N_{voxel} - 1} \right)^2 \tag{1}$$

where L is the length along one side of the square domain, while N_{voxel} is the number of voxels along the side of the domain. In this study, the number of voxels along each side was specified to be $N_{voxel} = 16$. While the voxel resolution in this study could be made

much finer to fully represent the wafer and pad surfaces, it does allow for a generalized prediction of the regions of local areas of contact, which can be used for the prediction of areas where surface wear takes place.

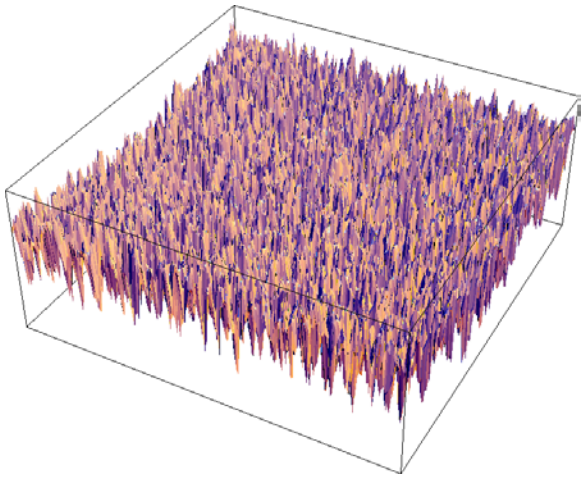

Figure 2a: Sample topography of the copper wafer that was used for the PAML simulations, measured using contact profilometry

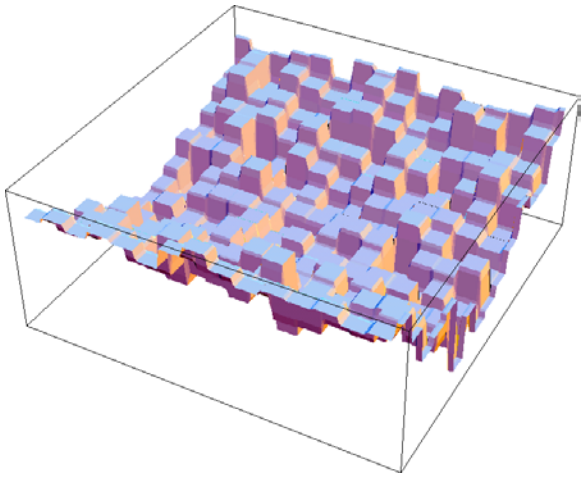

Figure 2b: Sample wafer surface topography represented as voxels ($N_x = N_y = 16$)

Past studies by Higgs and collaborators have used the voxel framework for modeling contact mechanics [21] and wear [22], respectively, between two mating surfaces. One

key advantage of using voxels in the PAML modeling approach is that they are a simplistic way of representing surfaces asperities so that they can interact with the particles *in silico*, namely in terms of the contact mechanics (see Section 4) and wear calculations (see Section 7). Consequently, the voxel framework was used in this study in order to employ simple, deterministic (topography-based) models into the contact mechanics and wear formulations. As discussed in Terrell and Higgs [21], this deterministic treatment of contacting surfaces can predict the distribution of contact stress, contact area [23], and wear.

3. Employing a PAML Approach to Simulating CMP

The PAML-based wear approach requires that one treats the contact mechanics, fluid mechanics, and the particle dynamics integrally in order to model the resulting wear of the surfaces. In this work, this was done using four key assumptions:

1. It was assumed that the asperities of the surfaces could be represented as voxels, as discussed in Section 2.
2. Since the area of interest in this study was significantly smaller than the scale of the wafer, it was assumed that the fluid pressure at the boundaries of the domain were equal.
3. The solid fraction of the slurry was assumed to be constant throughout the simulation.
4. The PAML approach assumed that a wear event occurred when a particle was trapped between the pad and wafer asperities.

After receiving the wafer and pad surface topographies as inputs, the PAML model simulated the contact mechanics, fluid mechanics, particle dynamics and wear that would occur if both of the surfaces were sliding against each other in the presence of slurry. The top (wafer) surface was specified to have the properties of a thin copper film, and had a normal load W applied in order to press it towards the pad. Although the wafer surface was specified with no horizontal velocity, it was actuated up and down in the vertical direction in order to balance the applied load W with the reaction force R, as discussed in Section 3. Meanwhile, the bottom (pad) surface was specified to translate

with a horizontal velocity $U = 0.4$ that is typical of the relative velocity in most CMP tests. The resulting wafer/pad domain is shown in Fig. 3. As the figure shows, the simulation was conducted over a square area with a side length of $L = 25$ μm. It must be noted that the wafer surface (shown upside down as a wireframe) appears to be flat in this image because its roughness is small compared to the roughness of the pad.

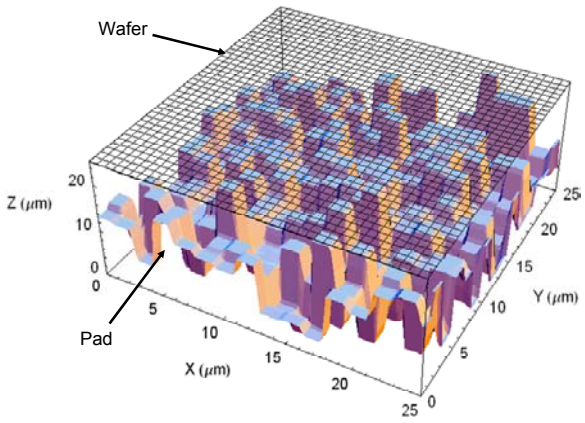

Figure 3: Diagram of the wafer/pad domain in one of the PAML simulations

A flowchart of the PAML simulation is shown in Fig. 4. The simulation begins by reading in a measured surface topography for the wafer and a randomly generated Gaussian pad topography. Particles are then seeded in the domain according to the specified solid fraction X, and the slurry velocity field is initialized to be zero everywhere in the domain. The simulation then begins stepping though time. Each of the time steps involves an update of the slurry velocity field (performed using the integrated CFD solver, described below), a calculation of the contact stress distribution between the two surfaces, an update of the locations and velocities of the abrasive particles, a calculation of the particle-induced wear at that time step, and then an advancement of the surface topographies according to their specified horizontal velocities (x- and y-movement), as well as the reaction force from the surface (z-movement).

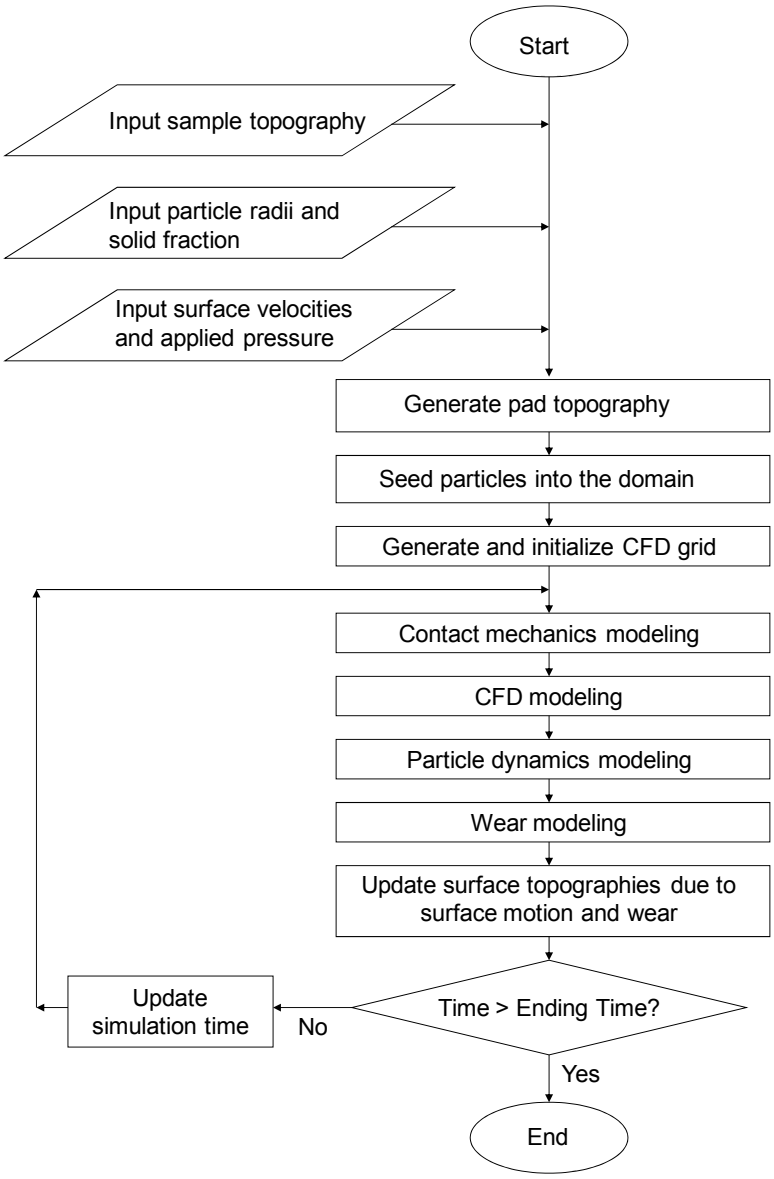

Figure 4: Flowchart of the PAML computational model

4. Contact Mechanics Modeling

The contact stress between the wafer and pad surfaces was modeled by treating the voxel asperities on both surfaces as independent, linear springs. The stress-deflection relationship for both surfaces was modeled using the 3D Hooke's Law model in the Winkler foundation [24], which is expressed as follows:

$$\sigma_i = \left(\frac{E(1-\nu)}{(1-2\nu)(1+\nu)t} \right) \Delta H_i = k \Delta H_i \text{ (individual voxel compression)} \quad (2)$$

where E is the elastic modulus, t is the thickness of the material, and ν is the Poisson's ratio of the material. The contact between the wafer and the pad was thus ultimately modeled as contact between a dual-layered "mattress" and a flat plane [25].

The PAML model accounted for plastic deformation by assuming that each of the voxels in the pad behaved as elastic-perfectly plastic springs, with the pad yield stress calculated according to the following [26]:

$$Y_{pad} = \frac{H_{pad}}{2.8} \tag{3}$$

where H_{pad} is the hardness of the pad surface. If the contact stress σ_i of any of the voxels in contact was found to be greater than the pad yield stress Y_p, then it was reset to be equal to the pad yield stress. Although a simplified model for plastic deformation was incorporated into the PAML model, the applied pressures were considered to be too small to cause significant material flow on a tribosystem-wide scale. Therefore, a complex material flow algorithm was not included in this model.

The reaction force R from the wafer-pad compression was calculated by summing up the stresses from all of the deflected voxels, then multiplying the total stress by the voxel area from Eq. (1) as follows:

$$R = A_{voxel} \sum_{i}^{Nvoxels} \sigma_i \tag{4}$$

As mentioned previously, the wafer surface was actuated in the z-direction in an attempt to reach force equilibrium. If the reaction force R was calculated to be less than the applied force W, then the top surface was lowered towards the pad at a specified velocity. If the reaction force was calculated to be greater than the applied force, then the top surface was raised away from the pad.

5. Fluid Mechanics Modeling

In order to solve the slurry flowfield in the wafer-pad gap, a number of CMP models [9, 27, 28] have employed the Reynolds equation, which neglects the inertial effects of the fluid. The Reynolds equation has been shown to be an effective way to predict the

hydrodynamic pressure in thin-film geometries. However, the authors believe that the need for a robust prediction of the slurry flowfield around the wafer and pad asperities in the PAML model requires the use of the full Navier-Stokes equations, which captures any inertial effects that may be caused by the movement of the fluid around the asperities.

The PAML model thus used an integrated 3D computational fluid dynamics (CFD) approach to solve for the fluid velocities $u(x,y,z,t)$, $v(x,y,z,t)$, and $w(x,y,z,t)$, as well as the pressure $p(x,y,z,t)$, inside the wafer-pad gap. Initial values of the fluid velocity and pressure were specified before the first time step of the simulation. After the simulation was started, the solver generated a structured fluid grid between the wafer and the pad asperities and updated the velocity flowfield and pressure field at each time step. It must be noted that the CFD simulation assumed the slurry fluid to be isothermal.

A diagram of the boundary conditions that were imposed in the PAML model is shown in Fig. 5. The location and motion of the pad and wafer asperities were incorporated as no-slip boundary conditions to the fluid, while the drag forces from the particles were imposed onto the fluid as discrete body forces. The sides of the domain in the positive-x, positive-y, negative-x, and negative-y directions were modeled as zero-gradient boundaries, so that fluid can travel into or out of the domain as necessary. The fluid pressure at each of the inflow/outflow boundaries was assumed to be equal in this study. Although a number of past studies have shown the fluid pressure to vary significantly across the length of the wafer-pad interface [15, 27, 28], the relatively small area (25 μm x 25 μm) of this study warranted the use of a constant-boundary-pressure assumption.

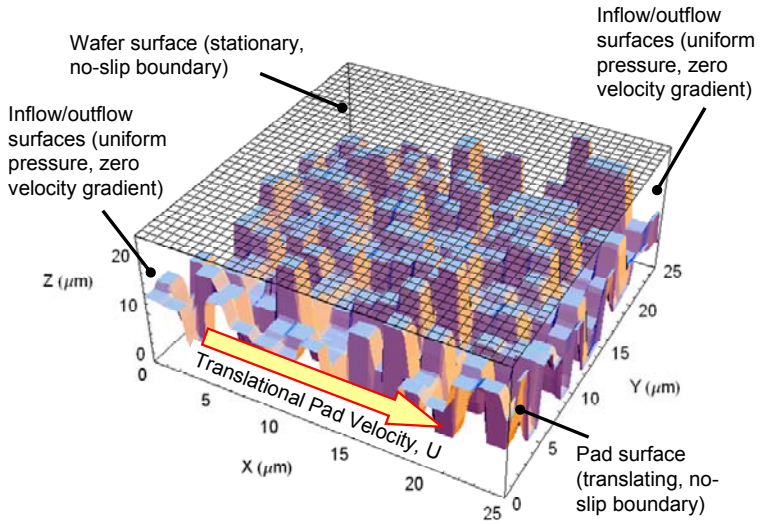

Figure 5: Diagram of the fluid boundary conditions that were implemented in the Chorin fluid flow solver

5.1. Solution Procedure: Chorin Projection Method

The CFD solver used the Chorin projection method [29] to solve the 3D, unsteady, isothermal, incompressible Navier-Stokes equations, given as follows:

$$\frac{\partial u}{\partial t}+\frac{\partial (u^2)}{\partial x}+\frac{\partial (uv)}{\partial y}+\frac{\partial (uw)}{\partial z}=-\frac{\partial p}{\partial x}+\frac{1}{Re}\left(\frac{\partial^2 u}{\partial x^2}+\frac{\partial^2 u}{\partial y^2}+\frac{\partial^2 u}{\partial z^2}\right)+g_x \tag{5a}$$

$$\frac{\partial v}{\partial t}+\frac{\partial (uv)}{\partial x}+\frac{\partial (v^2)}{\partial y}+\frac{\partial (vw)}{\partial z}=-\frac{\partial p}{\partial y}+\frac{1}{Re}\left(\frac{\partial^2 v}{\partial x^2}+\frac{\partial^2 v}{\partial y^2}+\frac{\partial^2 v}{\partial z^2}\right)+g_y \tag{5b}$$

$$\frac{\partial w}{\partial t}+\frac{\partial (uw)}{\partial x}+\frac{\partial (vw)}{\partial y}+\frac{\partial (w^2)}{\partial z}=-\frac{\partial p}{\partial z}+\frac{1}{Re}\left(\frac{\partial^2 w}{\partial x^2}+\frac{\partial^2 w}{\partial y^2}+\frac{\partial^2 w}{\partial z^2}\right)+g_z \tag{5c}$$

$$\frac{\partial u}{\partial x}+\frac{\partial v}{\partial y}+\frac{\partial w}{\partial z}=0 \tag{5d}$$

The CFD algorithm used in this study involved starting each time step with an initial guess of the velocity field, and then correcting the velocity field based upon the calculated pressure field. The velocities and pressures are specified on a structured, staggered three-dimensional grid, shown in Fig. 6. At each time step, the fluid velocities

u, *v*, and *w* from the previous time step are used to solve the Poisson pressure equation for the pressure field at the following time step. The Poisson pressure equation is solved using the successive over-relaxation (SOR) method, which iteratively updated the pressure field until the residuals of the Poisson equation fell below a tolerance of 1×10^{-3}. After the Poisson equation is solved, the velocity field is then updated from the calculated pressure field.

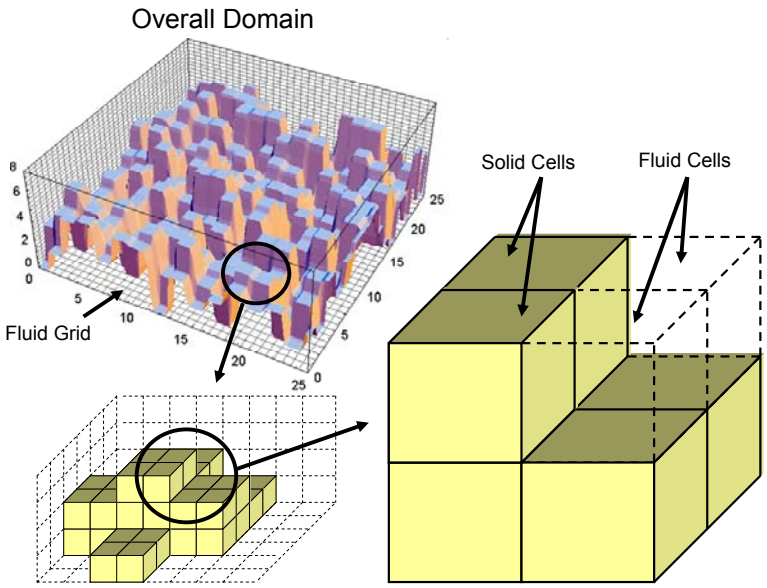

Figure 6: Diagram of the cell division of the PAML domain, which was used in the Chorin solver to solve the slurry flowfield

5.2. Grid Convergence Study

After the CFD code was developed, a series of transient lid-driven cavity simulations were performed with varying grid sizes in order to test for convergence in the CFD solver. From these simulations, the CFD module was shown to have 2nd order convergence. These results ensured that the CFD module could be integrated into the PAML algorithm.

6. Particle Dynamics Modeling

The motion of the abrasive particles in the slurry was tracked in a Lagrangian reference frame. In a manner similar to Terrell and Higgs [16], the motion of each particle was governed by the following dynamic equations:

$$\frac{dx_p}{dt} = u_p \tag{6a}$$

$$\frac{dy_p}{dt} = v_p \tag{6b}$$

$$\frac{dz_p}{dt} = w_p \tag{6c}$$

$$m_p \frac{du_p}{dt} = \sum f_{p,x} \tag{7a}$$

$$m_p \frac{dv_p}{dt} = \sum f_{p,y} \tag{7b}$$

$$m_p \frac{dw_p}{dt} = \sum f_{p,z} \tag{7c}$$

where m_p is the mass of the particle, and t is the time. Additionally, the parameters x_p, y_p, and z_p represent the location of the particle in each of the three principle directions, while u_p, v_p, and w_p denote the velocity of the particle in each direction. The applied forces on the particle in each direction are given by $f_{p,x}$, $f_{p,y}$, and $f_{p,z}$.

6.1. Applied Forces to Particles

Each of the particles was subject to applied forces from several different sources. These included gravitational and buoyancy forces, as well as Stokes drag force, hydrodynamic pressure force, and Saffman lift forces that were imposed due to the motion of the fluid. The drag and hydrodynamic pressure forces were applied in each of the three principal directions, while the Saffman lift, gravity, and buoyancy forces were only applied in the vertical (z) direction across the gap. A discussion of the mathematical formulation behind each of these forces is outlined in Terrell and Higgs [16]. While there is a body of work that suggests that the drag and Saffman lift forces in bounded flows may be altered [17, 30], the authors assumed that the standard relations as used in past studies [18, 19, 31] was sufficient given the complex geometries and interplay of multiple physics.

In addition to the gravitation, buoyancy, and fluid motion forces, the particles also experienced an impulse force whenever they collided with another particle or with one of the first-body surfaces. The collision impulse force was calculated based upon the assumption that the colliding particle would tend to have an instantaneous velocity change due to the collision if no other forces were present. The velocity change was calculated by combining the conservation of momentum and coefficient of restitution equations, given as follows:

$$m_1 v_1 + m_2 v_2 = m_1 v_1' + m_2 v_2' \tag{8a}$$

$$\varepsilon = \frac{v_2' - v_1'}{v_1 - v_2} \tag{8b}$$

where v_1 and v_1' are the pre- and post-collision velocities, respectively, of the first colliding object along the line of collision, while v_2 and v_2' are the pre- and post-collision velocities, respectively, of the second colliding object along the line of collision. In a similar approach to Terrell and Higgs [16], the coefficient of restitution was assumed to be zero for all collisions in this study, based upon the results of past studies [32, 33] that have tested the coefficient of restitution of colliding objects immersed in fluid. It must be noted that although the particle dynamics model in this study did not specifically account for atomic-scale forces on the abrasive particles, it is believed that these effects can be reasonably simulated by varying the coefficient of restitution.

After determining the instantaneous velocity change of the colliding objects, the impulse force for each colliding particle was calculated as follows:

$$f_{collision,x} = \frac{m_p (u_p' - u_p)}{\Delta t} \tag{9a}$$

$$f_{collision,y} = \frac{m_p (v_p' - v_p)}{\Delta t} \tag{9b}$$

$$f_{collision,z} = \frac{m_p (w_p' - w_p)}{\Delta t} \tag{9c}$$

where m_p is the mass of the particle and Δt is the size of the time step. If any particle was found to be in contact with another object during a given time step, the collision impulse force was calculated and added to the other applied forces that were acting on that particle at that time.

6.2 Simulation of Particle Motion

The velocity and position of each particle was updated at each time step by integrating the governing equations (Eqs. 6-7) according to the Verlet leapfrog scheme [34]. The Verlet scheme, a commonly-used algorithm in molecular dynamics simulations [34, 35], was used in this study due to its numerical accuracy. It must be noted that periodic boundary conditions were applied to the motion of the abrasive particles, in order to ensure that the number of particles in the domain remained constant.

6.3 The Particle-Induced Force on the Fluid

As mentioned previously, the applied force caused by an abrasive particle was imposed onto the fluid flowfield as a body force wherever a particle was located. This applied force was calculated as drag from the particle to the fluid as follows:

$$f_{fluid,x} = 6\pi a_p (u_p - u(x_p, y_p, z_p, t)) \tag{10a}$$

$$f_{fluid,y} = 6\pi a_p (v_p - v(x_p, y_p, z_p, t)) \tag{10b}$$

$$f_{fluid,z} = 6\pi a_p (w_p - w(x_p, y_p, z_p, t)) \tag{10c}$$

where a_p is the radius of the particle.

7. Wear Calculation

For this study, the authors assumed that the mechanical abrasive action from particle-surface sliding was the predominant enabling physics in CMP, and thus a wear event only occurred when an abrasive particle was trapped between wafer and pad asperities. This assumption follows the formulation of several other CMP studies [5, 8, 36], who have each found particle-based wear to be the primary wear mechanism in CMP. At each time step, the PAML simulation determined whether any particles were trapped in contact

between two contacting voxel asperities by identifying the surface asperities located immediately above and below each particle. If the diameter of any particle was larger than the gap that separated its surrounding surface asperities, then the particle-based wear was calculated.

The wear formulation in this study was based upon the prediction of a particle being effectively "scraped" into a voxel, and removing material due to abrasive wear, as shown in Fig. 7. The wear module in the PAML simulation thus functioned by first calculating the deflection of the particle into both surfaces, and then used the relative velocity between the particle and either surface in order to calculate the volume of the worn material from each contacting voxel. Although the wafer surface wear is the focus of this study, the PAML simulation also modeled the wear of the pad surface, which is considered to be a loss of conditioning roughness.

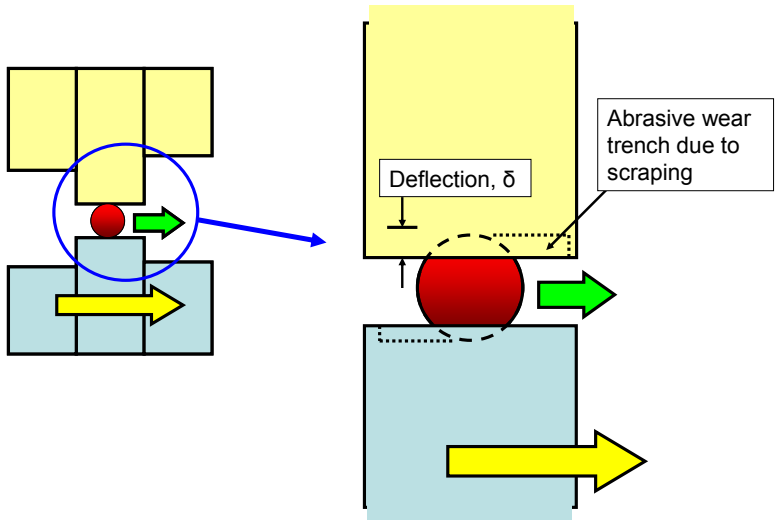

Figure 7: Diagram showing the basis of the wear formulation in this study, wherein a slurry particle digs a wear trench between the two contacting surfaces

If a particle was found to be trapped between voxel asperities in the wafer and the pad, the deflection δ of the particle into both surfaces was calculated according to Hertzian theory [26]. It must be noted that the PAML model assumed that each particle

experienced negligible deformation when being trapped between the wafer and pad asperities.

After calculating the deflection of each particle into the first-body surfaces, the reduction in voxel asperity height Δh due to particle-induced wear was calculated according to the abrasive wear formulation by Zhou and Chang [8]:

$$\Delta h = \frac{V \delta_p \Delta t \sqrt{2 \delta_p a_p}}{A_{voxel}} \tag{11}$$

where V is the relative sliding velocity between the particle and the surface, δ_p is the deflection of the particle into the surface, and a_p is the particle radius. Although Zhou and Chang specified a "critical" minimum deflection δ_{pc} that is necessary for plastic deformation and wear, it must be noted that the wear module in the first-generation PAML model assumed that wear would take place with both elastic and plastic deflection.

8. Simulation Parameters

The PAML model was implemented in the Mathematica® programming environment. Although a number of parameters can be extracted from the PAML simulation, this study focused on observing the predicted material removal rate (MRR) from the PAML simulation, and determining how the MRR changed with varying inputs. Therefore, a series of PAML simulations were conducted over an approximate simulated polishing time of t_{sim} = 30 μs, with each simulation specified with different parametric inputs. The base case was simulated with an applied pressure of W = 6 psi (41.4 kPa) and an abrasive particle radius a_p = 0.15 μm. Additionally, the particle solid fraction X, which is the ratio between the total volume of particles in the domain to the total volume of the slurry, was set to X = 4% for the base case which is consistent with commercial slurry. The other PAML cases were simulated with the applied pressure varying as W = [6 psi (41.4 kPa), 12 psi (82.7 kPa), 18 psi (124 kPa), 24 psi (166 kPa), 32 psi (221 kPa)], the solid fraction varying between X = [0.005, 0.01, 0.02, 0.03, 0.04], and the abrasive particle radius varying between a_p = [0.15 μm, 0.2 μm, 0.3 μm, 0.4 μm]. The remaining simulation parameters are given in Table 1.

Table 1: Input parameters used in PAML simulation

Parameter	Value
RMS roughness of pad (random Gaussian)	5 μm
Elastic modulus of pad, E_{pad}	300 MPa
Poisson's ratio of pad, v_{pad}	0.4
Hardness of pad, H_{pad}	5.0 MPa
Thickness of pad asperities, t_{pad}	10 μm
Elastic modulus of wafer (copper film), E_{wafer}	110 GPa
Poisson's ratio of wafer (copper film), v_{wafer}	0.16
Hardness of wafer (copper film), H_{wafer}	2 GPa
Thickness of wafer asperities, t_{wafer}	0.2 μm
Slurry density, ρ	1000 kg/m^3
Slurry viscosity, μ	0.001 kg/m-s
Radius of abrasive particles, a_p	0.15 μm
Density of abrasive particles, $\rho_{particle}$	2000 kg/m^3
Elastic modulus of the silica particles, $E_{particle}$	94 GPa
Poisson's ratio of the silica particles, $v_{particle}$	0.17
Number of voxels along each side of the domain, N_{voxels}	16
Relative velocity between pad and wafer, U	0.4 m/s

9. Experimental CMP Measurements

A series of in-house CMP tests were conducted in order to compare the measured wafer surface wear with the predictions from the PAML simulations. All of the CMP tests were conducted using a Strasbaugh 6CA polisher. The polisher, which had a 22" diameter platen, was fitted with a porous polyurethane FastPad® donated by PPG Industries. The pad featured concentric grooves in order to assist with slurry transport to the wafer. The slurry that was used in this study was Semi-Sperse® 25E, donated by Cabot Microelectronics. The slurry was diluted according to the manufacturer's specifications, such that the resultant solid fraction of the abrasive silica particles was X = 4%. According to the manufacturer, the mean radius of the abrasive particles in the slurry was a_p = 0.15 μm.

This experimental study involved the polishing of five different copper wafers, each for a time period of t_{polish} = 30 sec. All of the polish runs involved a wafer and pad rotational speed both equal to $N_{wafer} = N_{pad}$ = 32 RPM. The wafer/pad relative velocity was U = 0.4 m/s at a radial location of r = 2.2 cm from the center of the wafer. Each of the wafers was polished with a different applied pressure, in order to compare with the parametric results of the PAML simulations. The applied pressures for these tests were W = [6 psi (41.4 kPa), 12 psi (82.7 kPa), 18 psi (124 kPa), 24 psi (166 kPa), 32 psi (221 kPa)].

After polishing, a trench was etched into the copper surfaces of each of the five polished wafers. This was performed by applying a small line of nitric acid across the length of the wafer surface using a cotton swab. In addition, a sixth wafer, which was not polished using the Strasbaugh, was also etched in the same manner as the five polished wafers. After etching, the step heights of all six wafers were measured using a Wyko optical profilometer. These measurements were conducted at an approximate radius of r = 2 cm from the center of each wafer. A sample step height measurement is shown in Fig. 8.

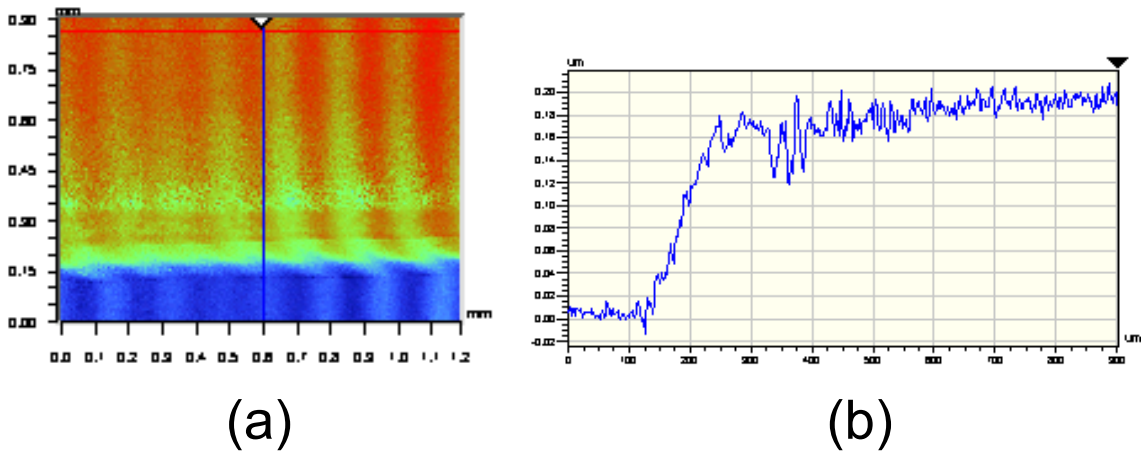

Figure 8: Sample step height measurement of copper film wafer—(a) contour plot, (b) line plot across center of plot

The step height measurement from the unpolished wafer was used as the starting thickness of all of the polished copper films, under the assumption that all of the wafers in the batch were deposited similarly. The resultant MRR for each of the polished wafers was calculated according to the following:

$$MRR_{measured} = \frac{h_{unpolished} - h_{polished}}{t_{polish}} \tag{12}$$

10. Results and Discussion

The predicted wear from the PAML simulations are compared to the measured wear from experimental CMP in this section. This section also shows the variation in predicted MRR when the slurry solid fraction and abrasive particle size are varied.

10.1. PAML Wear Prediction

Figure 9 shows the predicted PAML domain at an instance of time. During each time step, the simulation identified which particles were involved in a wear event, and calculated the resulting wear volume.

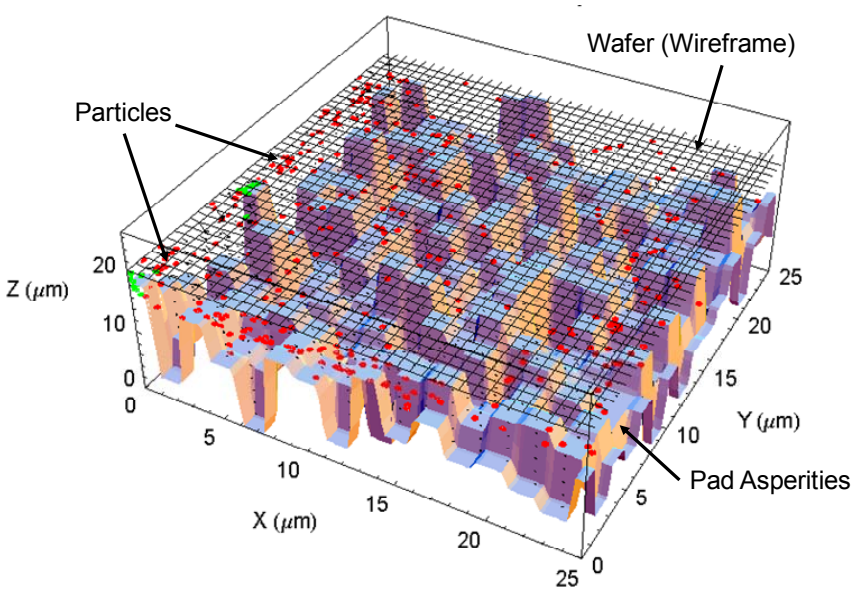

Figure 9: PAML simulation at a given instance in time.

The MRR of the wafer surface was observed for each of the PAML simulations. The instantaneous and cumulative wear from the wafer surface as a function of time for the base case are shown in Figs. 10 and 11, respectively. It is clearly seen from these figures that the wear is discrete in both space and time, since it is dependent on the abrasive contact of the particles between the wafer and pad asperities.

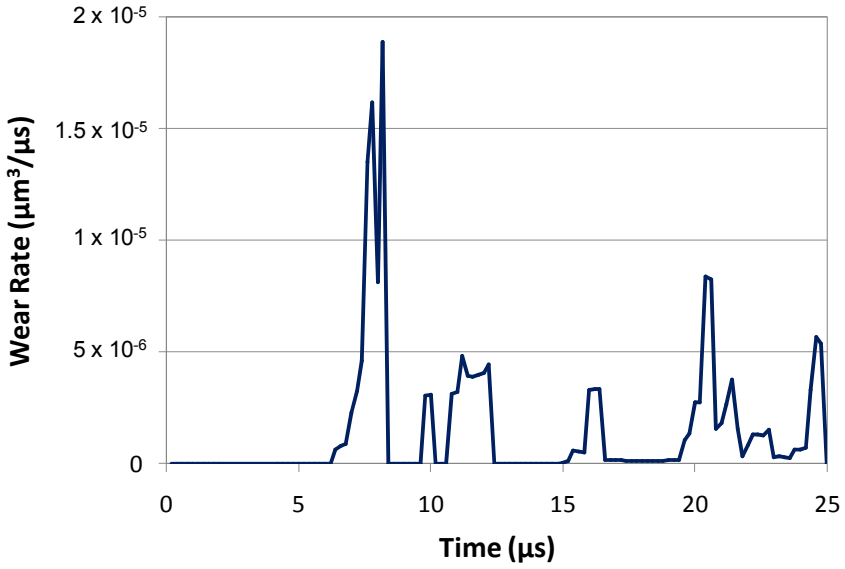

Figure 10: PAML prediction of the instantaneous wear of the wafer surface for the base case (W = 6 psi, X = 0.04, a_p = 0.15 µm)

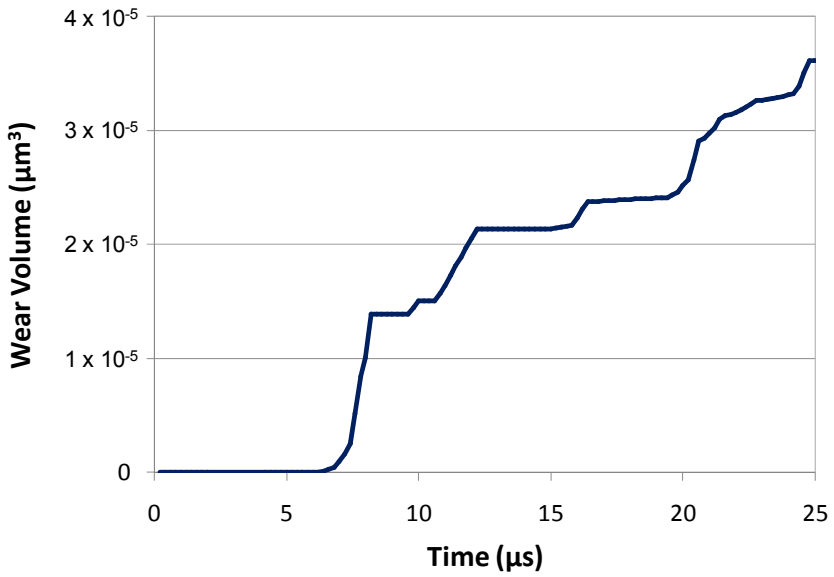

Figure 11: PAML prediction of the cumulative wear of the wafer surface for the base case (W = 6 psi, X = 0.04, a_p = 0.15 µm)

10.2. PAML-Experiment Comparison

Figure 12 shows the predicted wear rate from the PAML simulations compared to the measured wear from in-house CMP experimentation. Both the predicted and measured MRR show similar trends with varied pressure, with the MRR mostly increasing as the applied pressure is increased. The main exception in this trend involves the MRR that was observed at an applied pressure of 12 psi, which decreased slightly from the MRR that was measured/predicted at 6 psi. It can be observed from this comparison that the predicted MRR diverges increasingly from the measured MRR as the applied pressure is increased. This indicates that a refinement of the wear event criterion in PAML may be necessary to reduce the wear sensitivity at high applied loads.

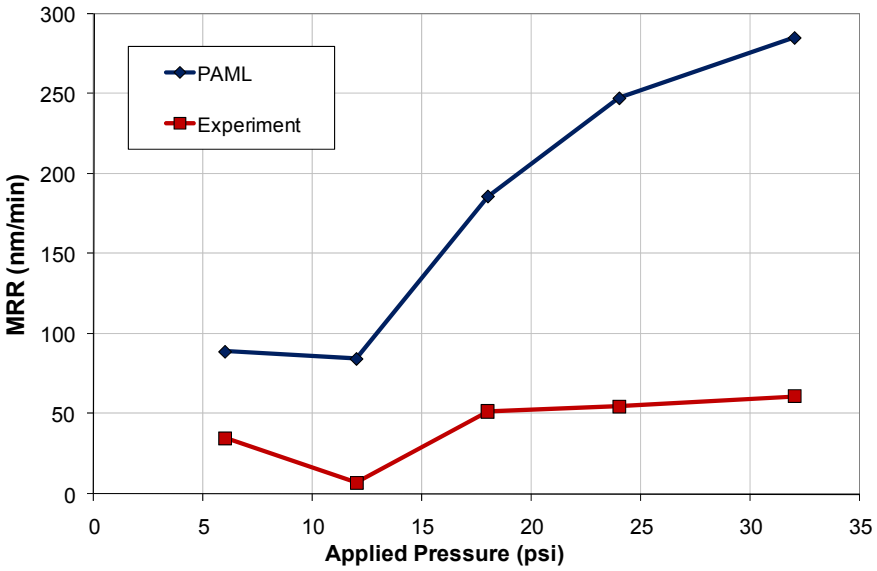

Figure 12: Comparison between predicted and measured MRR

Although the trends in the predicted and measured MRR were similar to each other, Fig. 12 shows that the PAML predicted MRR was at least twice as large as the measured MRR. This difference can be attributed to a number of factors. First, the length and time scale differences between the model and experiment were of several orders of magnitude, and should have caused a discrepancy between the experimental and predicted results. Additionally, because the PAML model was simulated over a relatively short timeframe, its predictions may have been reflecting the "run-in" physics that is required for the system to reach a quasi-steady-state wear rate. In most tribological systems, the initial wear is relatively large compared to the steady-state wear rate due to the wear-in of the initial topographies of both surfaces [37]. Other researchers such as Chandra and collaborators [7] have even developed theory aimed at reducing the magnitude of the MRR predicted by particle-induced abrasive wear models. A fourth possible reason for the modeling/experimental discrepancy involves the hardness and microstructure variations in the surfaces of the wafers. This variation may not have been adequately captured in the current PAML model, although it is believed that the model can be easily modified in order to accommodate microstructure. Finally, the discrepancy between model and experiment may also be attributed to the rolling contact of the abrasive

particles against the surface asperities. Because the PAML model assumed that all particles that were trapped between two asperities caused sliding wear, the lack of rolling contact prediction is an additional reason as to why the PAML wear predictions are larger than experimental measurements.

10.3. Variation in PAML-predicted MRR with Different Parametric Inputs

A series of additional PAML simulations were conducted with various inputs in order to test the predictive capability of the model with various parameters. These parametric studies involved the variation of the particles' mechanical properties, the particle solid fraction X, and the particle radius a_p.

The PAML-predicted variation in MRR with particle solid fraction X is shown in Fig. 13. It can be observed that the predicted MRR tends to increase as the solid fraction is increased. A similar trend was found from the experimental CMP measurements of Bielmann et al. [38] This phenomenon is expected, as increasing the number of particles in the domain should provide a greater chance of abrasive contact of a particle between the wafer and pad surfaces, and an increased amount of wear.

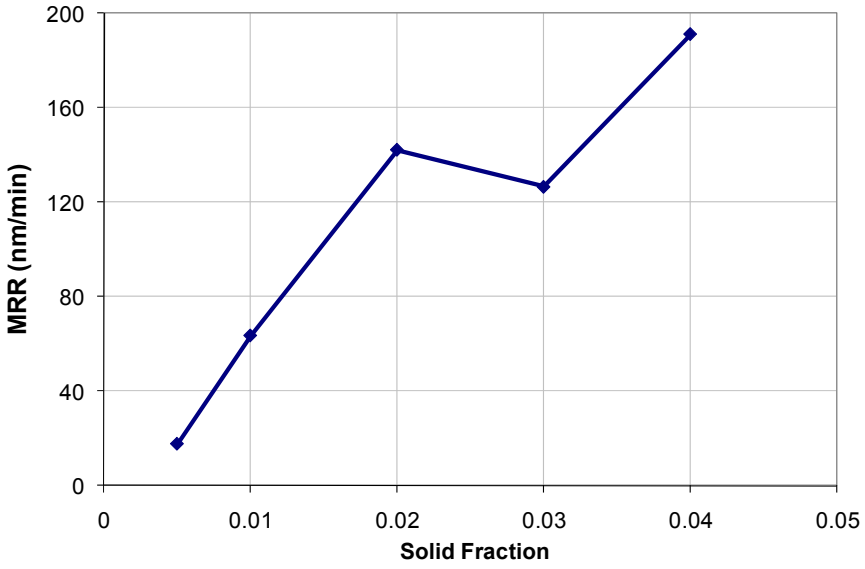

Figure 13: PAML prediction of MRR with varied inputs for particle solid fraction

Figure 14 shows the PAML prediction of MRR as a function of abrasive particle radius a_p. This figure appears to show that the predicted wear decreases as the particle radius is increased. Similar trends have been found from the experimental measurements of Bielmann et al. [38], as well as the model predictions of Luo and Dornfield [39]. The prediction of decreasing MRR with increasing abrasive particle size is intuitive in consideration of the wear formulation that is discussed in Section 7. When involved in surface contact, larger particles have larger contact areas and thus apply smaller local contact pressures, which results in less wear.

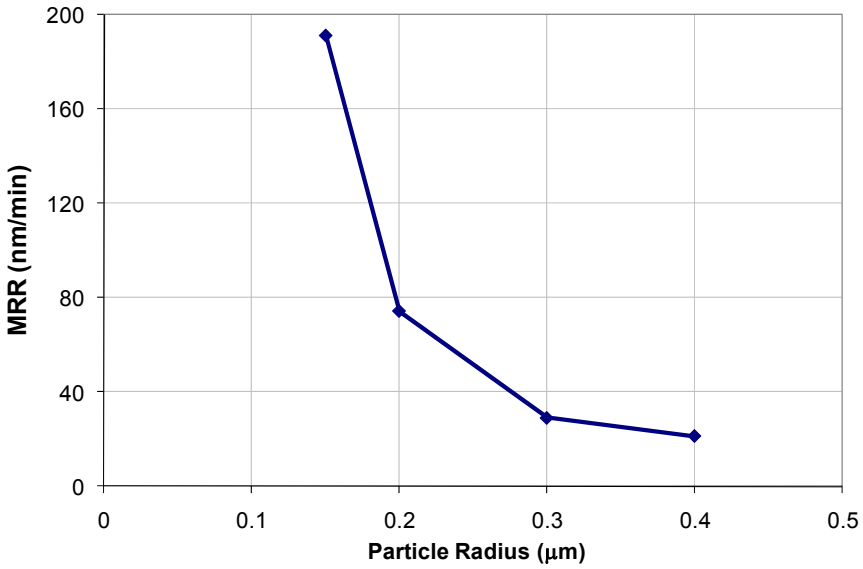

Figure 14: PAML prediction of MRR with varied inputs for abrasive particle radius

11. Conclusion

A multi-physics model of particle augmented mixed lubrication (PAML) was developed in order to predict the integrated contact mechanics, fluid mechanics, particle dynamics, and wear phenomena occurring during CMP. In order to reduce uncertainty in predicting the evolution of the thin film wafer surface, the actual deterministic surface topography of the wafer was used as input. Additionally, a CMP pad surface was generated according to the statistics of an actual commercial pad surface in order to accurately model the contact mechanics and wear of the wafer/pad sliding contact. The evolving interface was simultaneously used as input into the full isothermal, 3D multiphase slurry solution

consisting of both particle and fluid phases. Since a wear event only occurred when an abrasive particle is in contact with both the wafer and pad surfaces, the simulation showed that wear was intermittent and discrete in both space and time. While the PAML model over-predicted the experimental MRR, it did follow a similar trend to the experimentally measured MRR. It is believed that the model will be greatly improved with more refined property inputs, possible refinements to its wear formulation, and an increase in simulation length and time scales. Parametric studies showed that the PAML model predicted that the MRR increases almost monotonically as the particle solid fraction is increased, and decreases as the particle radius is increased. Both of these predictions are consistent with previously published results from the literature and are tribologically intuitive when considering various aspects of the wear phenomena that occur in CMP. Since CMP is predominantly governed by PAML phenomena, this work serves as a testbed for employing a PAML modeling approach to predict similar problems found in tribology.

Acknowledgements

The authors gratefully acknowledge the support of the Alfred P. Sloan Foundation, the Society for Manufacturing Engineers (SME), the Pennsylvania Infrastructure Technology Alliance (PITA), and the NSF CAREER program within the CMMI division. Additionally, the authors acknowledge in-kind contributions from PPG, Cabot Microelectronics, and AMS. The authors also thank Prof. S. Balachandar from the University of Florida for comments on studies involving particle forces. Lastly, the authors would like to thank the members of the Particle Flow and Tribology Laboratory at Carnegie Mellon for their scholarly input in this work, namely Joseph Bonivel, Venkata Jasti, Jeremiah Mpagazehe, and Emmanuel Wornyoh.

References

[1] Nanz, G., and Camilletti, L. E., 1995, "Modeling of Chemical-Mechanical Polishing - a Review," IEEE Transactions on Semiconductor Manufacturing, 8(4), pp. 382-389.

[2] Zantye, P. B., Kumar, A., and Sikder, A. K., 2004, "Chemical Mechanical Planarization for Microelectronics Applications," Materials Science and Engineering R: Reports, 45(3-6), pp. 132.
[3] Castillo-Mejia, D., and Beaudoin, S., 2003, "A Locally Relevant Prestonian Model for Wafer Polishing," J. of the Electrochemical Society, 150(2), pp. G96-G102.
[4] Seok, J., Sukam, C. P., Kim, A. T., Tichy, J. A., and Cale, T. S., 2003, "Multiscale Material Removal Modeling of Chemical Mechanical Polishing," Wear, 254(3-4), pp. 307-320.
[5] Luo, J. F., and Dornfeld, D. A., 2001, "Material Removal Mechanism in Chemical Mechanical Polishing: Theory and Modeling," IEEE Transactions on Semiconductor Manufacturing, 14(2), pp. 112-133.
[6] Zeng, T. F., and Sun, T., 2005, "Size Effect of Nanoparticles in Chemical Mechanical Polishing - a Transient Model," IEEE Transactions on Semiconductor Manufacturing, 18(4), pp. 655-663.
[7] Che, W., Guo, Y. J., Chandra, A., and Bastawros, A., 2005, "A Scratch Intersection Model of Material Removal During Chemical Mechanical Planarization (Cmp)," J. of Manufacturing Science and Engineering, 127(3), pp. 545-554.
[8] Zhao, Y. W., and Chang, L., 2002, "A Micro-Contact and Wear Model for Chemical-Mechanical Polishing of Silicon Wafers," Wear, 252(3-4), pp. 220-226.
[9] Lin, J. F., Chern, J. D., Chang, Y. H., Kuo, P. L., and Tsai, M. S., 2004, "Analysis of the Tribological Mechanisms Arising in the Chemical Mechanical Polishing of Copper-Film Wafers," J. of Tribology, 126(1), pp. 185-199.
[10] Ouma, D. O., Boning, D. S., Chung, J. E., Easter, W. G., Saxena, V., Misra, S., and Crevasse, A., 2002, "Characterization and Modeling of Oxide Chemical-Mechanical Polishing Using Planarization Length and Pattern Density Concepts," IEEE Transactions on Semiconductor Manufacturing, 15(2), pp. 232-244.
[11] Chekina, O. G., Keer, L. M., and Liang, H., 1998, "Wear-Contact Problems and Modeling of Chemical Mechanical Polishing," J. of the Electrochemical Society, 145(6), pp. 2100-2106.

[12] Terrell, E. J., and Higgs, C. F., 2006, "Hydrodynamics of Slurry Flow in Chemical Mechanical Polishing - a Review," J. of the Electrochemical Society, 153(6), pp. K15-K22.
[13] Runnels, S. R., 1994, "Feature-Scale Fluid-Based Erosion Modeling for Chemical-Mechanical Polishing," J. of the Electrochemical Society, 141(7), pp. 1900-1904.
[14] Yao, C. H., Feke, D. L., Robinson, K. M., and Meikle, S., 2000, "Modeling of Chemical Mechanical Polishing Processes Using a Discretized Geometry Approach," J. of the Electrochemical Society, 147(4), pp. 1502-1512.
[15] Higgs, C. F., Ng, S. H., Borucki, L., Yoon, I., and Danyluk, S., 2005, "A Mixed-Lubrication Approach to Predicting Cmp Fluid Pressure Modeling and Experiments," J. of the Electrochemical Society, 152(3), pp. 193-198.
[16] Terrell, E. J., and Higgs, C. F., 2007, "A Modeling Approach for Predicting the Abrasive Particle Motion During Chemical Mechanical Polishing," J. of Tribology, 129(4), pp. 933 - 941.
[17] Shen, X., and Bogy, D. B., 2003, "Particle Flow and Contamination in Slider Air Bearings for Hard Disk Drives," J. of Tribology, 125(2), pp. 358-363.
[18] Zhang, S., and Bogy, D. B., 1997, "Effects of Lift on the Motion of Particles in the Recessed Regions of a Slider," Physics of Fluids, 9(5), pp. 1265.
[19] Terrell, E. J., and Higgs Iii, C. F., 2007, "A Simulation of Contaminates around the Solid Immersion Lens in a near-Field Optical Recording System," IEEE Transactions on Magnetics, 43(3), pp. 1086 - 1092.
[20] Sieburg, H. B., 1990, "Physiological Studies *in Silico*," Studies in the Sciences of Complexity, 12, pp. 321-342.
[21] Terrell, E. J., and Higgs, C. F., 2006, "Contact Stress Analysis of Thin Film Compression: Modeling, Simulation, and Experiment," ASME Paper IJTC2006-12300.
[22] Terrell, E. J., Kuo, M., and Higgs, C. F., 2007, "An Approach to Modeling Particle-Based and Contact-Based Wear in Cmp," Proceedings of the Materials Research Society Symposium C, 991.
[23] Dickrell, D. J., Dugger, M. T., Hamilton, M. A., and Sawyer, W. G., 2007, "Direct Contact-Area Computation for Mems Using Real Topographic Surface Data," Journal of Microelectromechanical Systems, 16(5), pp. 1263 - 1268.

[24] Jin, X., Keer, L. M., and Wang, Q., 2005, "A 3d Ehl Simulation of Cmp: Theoretical Framework of Modeling," J. of the Electrochemical Society, 152(1), pp. 7-15.
[25] Terrell, E. J., Kuo, M., and Higgs, C. F., 2007, "An Approach to Modeling Particle-Based and Contact-Based Wear in Cmp," Proceedings of the Materials Research Society Symposium, 991.
[26] Johnson, K. L., 1985, *Contact Mechanics*, Cambridge University Press, Cambridge.
[27] Shan, L., Levert, J., Meade, L., Tichy, J., and Danyluk, S., 2000, "Interfacial Fluid Mechanics and Pressure Prediction in Chemical Mechanical Polishing," J. of Tribology, 122(3), pp. 539-543.
[28] Sundararajan, S., Thakurta, D. G., Schwendeman, D. W., Murarka, S. P., and Gill, W. N., 1999, "Two-Dimensional Wafer-Scale Chemical Mechanical Planarization Models Based on Lubrication Theory and Mass Transport," J. of the Electrochemical Society, 146(2), pp. 761-766.
[29] Chorin, A. J., 1968, "Numerical Solution of Navier-Stokes Equations," Mathematics of Computation, 22(104), pp. 745 - 762.
[30] Cherukat, P., and Mclaughlin, J. B., 1994, "Inertial Lift on a Rigid Sphere in a Linear Shear Flow Field near a Flat Wall," J. of Fluid Mechanics, 263, pp. 1-18.
[31] Zhang, S., Wang, L., Jones, P., and Lopatin, G., 1999, "Numerical and Experimental Study of the Particle Contamination in a Head/Media Interface," IEEE Transactions on Magnetics, 35(5 pt 1), pp. 2442-2444.
[32] Joseph, G. G., Zenit, R., and Hunt, M. L., 2001, "Particle-Wall Collisions in a Viscous Fluid," J. of Fluid Mechanics, 433(1), pp. 329 - 346.
[33] Gondret, P., Lance, M., and Petit, L., 2002, "Bouncing Motion of Spherical Particles in Fluids," Physics of Fluids, 14(2), pp. 643-652.
[34] Frenkel, D., and Smit, B., 2002, *Understanding Molecular Simulations: From Algorithms to Applications*, Academic Press, Inc., Orlando, FL.
[35] Thomas, J. A., and Mcgaughey, A. J. H., 2007, "Effect of Surface Wettability on Liquid Density, Structure, and Diffusion near a Solid Surface," J. of Chemical Physics, 126(3), pp. 034707.
[36] Larsen-Basse, J., and Liang, H., 1999, "Probable Role of Abrasion in Chemo-Mechanical Polishing of Tungsten," Wear, 233-235, pp. 647-654.

[37] Totten, G. E., and Liang, H., 2004, *Mechanical Tribology: Materials, Characterization, and Applications*, Marcel Dekker, New York, NY.

[38] Bielmann, M., Mahajan, U., and Singh, R. K., 1999, "Effect of Particle Size During Tungsten Chemical Mechanical Polishing," Electrochemical and Solid State Letters, 2(8), pp. 401-403.

[39] Luo, J., and Dornfeld, D. A., 2003, "Effects of Abrasive Size Distribution in Chemical Mechanical Planarization: Modeling and Verification," IEEE Transactions on Semiconductor Manufacturing, 16(3), pp. 469-476.